Available online at www.sciencedirect.com
SCIENCE DIRECT®
Physics of the Earth and Planetary Interiors 154 (2006) 276–289
PHYSICS OF THE EARTH AND PLANETARY INTERIORS
www.elsevier.com/locate/pepi

Magnetic properties of olivine basalt: Application to Mars

H.P. Gunnlaugsson[a,*], Ö. Helgason[b], L. Kristjánsson[b], P. Nørnberg[c], H. Rasmussen[c], S. Steinþórsson[b], G. Weyer[a]

[a] *Institute of Physics and Astronomy, Aarhus University, Ny Munkegade, DK-8000 Århus C, Denmark*
[b] *Science Institute, University of Iceland, Dunhaga 3, IS-107 Reykjavík, Iceland*
[c] *Department of Earth Sciences, Aarhus University, Ny Munkegade, DK-8000 Århus C, Denmark*

Received 29 November 2004; received in revised form 15 September 2005; accepted 7 November 2005

Abstract

The natural remanent magnetisation (NRM) of basalt lava containing (oxidised) magnetic phases is usually assumed to be proportional to the weight percent of magnetic phases. It is shown here that olivine basalt has a different behaviour. The NRM intensity increases at an increasing rate with the amount of magnetic phases. This is attributed to the oxidation of olivine during cooling of the basalt that leads to the exsolution of magnetite in a single domain state. In this way, olivine basalt is found to become an order of magnitude more magnetic than basalt that does not contain olivine. A simple explanation for the magnetic anomalies on Mars is offered, based upon these findings and Mössbauer spectroscopy data from Gusev crater on Mars.

Keywords: Olivine basalt; NRM; Mössbauer spectroscopy; Mars; Magnetic anomalies; Icelandic basalt

1. Introduction

The natural remanent magnetisation (NRM) observed for basaltic lavas depends upon a number of conditions. Crucial parameters include the intensity of the external magnetic field during solidification, the chemistry of the lava, oxygen fugacity, cooling rate and its history after solidification, e.g. effects of any reheating and chemical alteration. Within a single lava flow, significant variations in the NRM are often observed. By examining a number of samples from the same flow, many of the parameters affecting the NRM can be kept constant. Here are presented the results of a detailed study of a number of lavas from Iceland, ranging in age from 3 to 16 My.

The NRM intensity can give information on the properties of the basalt during solidification. For single-domain (SD) magnetite, the thermal remanent magnetisation (TRM) obtained in ∼50 μT field is of the order 10^{-2} of the saturation value (σ_r/σ_S), compared to 10^{-3} for multi-domain (MD) magnetite (see e.g. the data from Kletetschka et al., 2000, 2005; Dunlop, 1990). In the former case, the TRM of the magnetite (by volume) will be of the order of $M_{r,mag}$ = 2000–3000 A/m, while in the latter case a value of $M_{r,mag}$ = 200–300 A/m is typical.

To get in-depth information on the magnetic properties of a sample, it is necessary to determine its mineralogy and the amount of magnetic phases in particular. To do this, Mössbauer spectroscopy has been applied, which is an ideal method to characterise the iron mineralogy of natural samples. Simultaneously information on the valence state of iron, magnetic interactions and site symmetry is obtained. Using a combination of

* Corresponding author. Tel.: +45 89423723; fax: +45 86120740.
E-mail address: hpg@phys.au.dk (H.P. Gunnlaugsson).

0031-9201/$ – see front matter © 2006 Elsevier B.V. All rights reserved.
doi:10.1016/j.pepi.2005.09.012

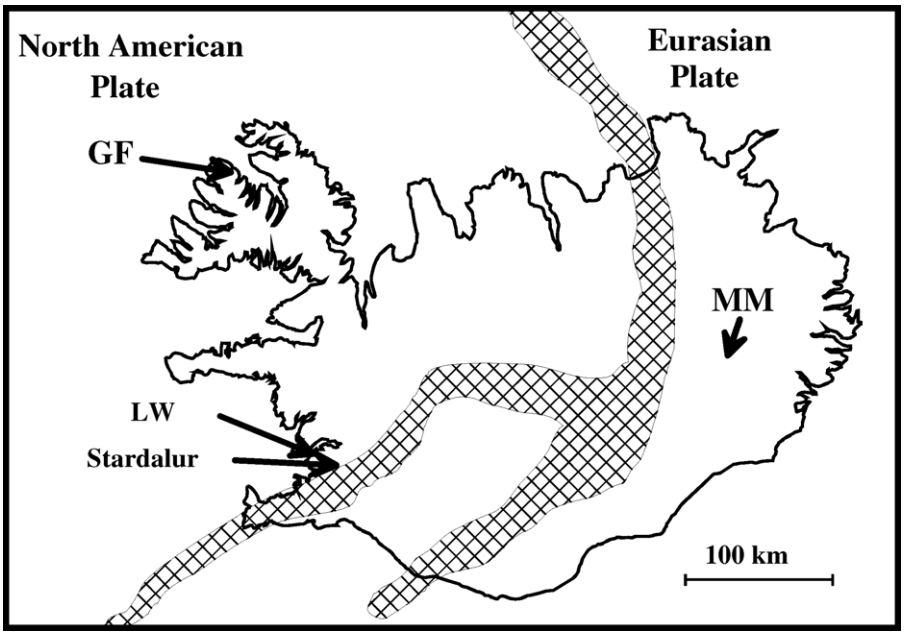

Fig. 1. Map of Iceland. The cross-shaded area represents the active rift zone, and arrows point to the sampling sites.

techniques, as described below, it is possible to determine the amount of iron-bearing phases with good accuracy.

A systematic study of the magnetic properties and Mössbauer spectra of Icelandic basalts has been conducted over the last few decades. This work has revealed a general trend associated with the ageing and alteration of basalt from the fresh rocks at the median rift zone where they are formed (cf. Fig. 1) to the east and west coasts (age up to ∼16 My). The kinematics of crustal spreading cause the basalts at the rift zone to be buried by younger formations, reheated and carried outwards towards the coasts where they have been exposed by glacial erosion. The degree of alteration at the base of the lava succession corresponds generally to maximum temperatures of <200 °C (e.g. Ade-Hall et al., 1971; Mehegan et al., 1982).

The main bulk of fresh basaltic lavas contain titanomagnetite ($Fe_{3-x}Ti_xO_4$) with relatively high values of x, typically $x = 0.6$–0.7 (Curie temperatures, $T_C = 0$–200 °C) whereas the altered basalts have T_C approaching 580 °C indicating a very low x (Becker, 1980). This compositional change is brought about by low-temperature solvus exsolution (as opposed to high-temperature oxy-exsolution) in the titanomagnetite (Vincent et al., 1957; Hoblitt and Larson, 1975; Steinthorsson et al., 1992). Oxidation of the titanomagnetite may lead to the formation of maghemite (γ-Fe_2O_3) (Steinthorsson et al., 1992) and finally, by inversion, to hematite (Gunnlaugsson et al., 2002).

Pure magnetite can also form upon oxidation of olivine during the solidification of the basalt and/or later oxidation (Haggerty and Baker, 1967; Hoye and Evans, 1975; Hoffmann and Soffel, 1986). The end product of the processes depends on various parameters such as oxygen fugacity, annealing temperature and time and the mineralogy of the parent material. These conditions determine in particular whether hematite or magnetite is formed, and the mineralogy of the silicate phases formed. Under the microscope, several characteristics have been observed: formation of iron oxides on the surface of the original olivine particles (diffusion rims) (Haggerty and Baker, 1967), and iron oxides imbedded as small particles in the silicate matrix, the shape and size of which depends on the formation conditions (Hoye and Evans, 1975).

In this study, we concentrate on samples of olivine basalt of high NRM intensity. Aeromagnetic surveys over Iceland have revealed a large number of distinctly localized magnetic anomalies (Kristjansson, 1970; Sigurgeirsson, 1970; Jonsson et al., 1991). They are less extensive than their Martian counterparts and usually associated with volcanic centres or subglacial volcanism. In some cases, access to the magnetic rocks has been obtained, either through erosion or by drilling.

Basalt lavas from Iceland are usually either magnetised normally, i.e. solidified in a magnetic field with geomagnetic pole at a similar location as to present location, giving rise to a positive magnetic anomaly, or reversely

magnetised giving rise to a negative anomaly. The current geomagnetic field over Iceland is about 51 μT and +75° tilt. In 1 km altitude, local anomalies with residual magnetic field of 1–2 μT are common (Jonsson et al., 1991).

2. Samples

Some of the samples that have been used for this study were sampled more than three decades ago (Stardalur samples). In this study, these have been revisited both because of the large amount of data that exist on them, their special properties, and the fact that new technology allows for a deeper study of their properties. A study like this is hampered by the fact that the occurrence of highly magnetic rocks is rare, and we have only a limited number of samples. The data used in this study represent all available data on highly magnetic rocks that cannot be explained by simple quenching of the basalt.

The samples used in this study were mostly drill cores (∼11 cm^3) collected for paleomagnetic measurements. Pieces of the samples were polished and carbon coated for scanning electron microscopy (SEM) studies, and the rest ground to homogeneous powder with an average particle size ∼50 μm for use in all other types of measurements. Magnetic separates were obtained by placing the powder sample on a piece of paper and applying hand magnets to extract the most magnetic particles.

The term olivine basalt is used here as determined by Mössbauer spectroscopy with the following criteria: if the area fraction of Fe(II) in olivine is larger than 10% of the silicate phases (Fe(III), Fe(II) in pyroxene and Fe(II) in olivine), we choose to call the samples olivine basalt.

2.1. Stardalur samples

The farm Stardalur is located 20 km northeast of Reykjavík (cf. Fig. 1). Aeromagnetic surveys revealed a positive magnetic anomaly, roughly 2 km × 2 km in dimension with a surface residual magnetic field as high as 28 μT (Friðleifsson and Kristjansson, 1972). A drilling project was undertaken in the 1970s to gain access to the magnetic rocks and seek answers regarding the source of the anomaly (Steinthorsson and Sigvaldason, 1971). The top 41 m consist of olivine tholeiite lava and breccia of low NRM intensity. Further down, highly magnetic early Quaternary lavas extending to depths of at least 140 m were drilled. The NRM intensity of these rocks was found to be M_r = 61 A/m on the average. The inclination of the stable NRM component in over 100 m of drill core was found to be 81°, with a standard deviation of 4° which is much lower than generally observed in Icelandic lava successions (Friðleifsson and Kristjansson, 1972; Kristjansson et al., 2003). This indicates that the lava pile in Stardalur was emplaced within a time interval of the order of a few centuries or less. The fact that the NRM directions in the Stardalur samples have unusually little scatter, also indicates that the intensity of any drilling-induced remanence is very minor compared to that of the NRM.

There are several factors that make the Stardalur samples special in this context. First of all, the magnetic phase is pure magnetite (Helgason et al., 1990), often found in submicron lamellae together with ilmenite, originating from solvus-exsolution of the original titanomagnetite (Steinthorsson and Sigvaldason, 1971). This is not uncommon, but cases of total absence of further oxidation products such as maghemite and hematite are very unusual in Icelandic basalt. Furthermore, the rocks were found to be rather iron rich (∼12 wt.% Fe), which is not anomalous but an unusually large proportion of the iron was situated in magnetite, or roughly 30% of the area of the Mössbauer spectra, while 5–10% is more usually the case.

2.2. Bolungarvík samples (GF)

The site called Bolungarvík is situated in the Tertiary NW part of Iceland (cf. Fig. 1), which is mainly built up of flood basalts representing the oldest exposed rocks in Iceland (14–16 My).

During field work at the mountain Tradarhyrna close to the village Bolungarvík, samples were taken from 26 lava flows (GF26 on top) and investigated for their magnetic properties and NRM direction (Kristjansson et al., 2003). Usually, four or five samples were taken from each lava. Three of the lavas (GF20–GF22) contained samples of unusually high NRM intensity (M_r up to ∼60 A/m).

Although this suggests heterogeneous rocks in terms of magnetic properties, these three lavas form a large part of our available data set, and show all the properties observed in other units.

2.3. Sudurdalur samples (MM)

The MM samples come from Sudurdalur, East Iceland (Kristjansson and Guðmundsson, 2005) from roughly 7 My old rocks (cf. Fig. 1). The samples used in this study come from two different lava flows, marked MM1-4 and MM2-4. This is of course a drawback in a comparative study. However, these two lavas/samples are chemically alike but differ by a factor of 10 in NRM intensity, being 4

and 40 A/m for MM1-4 and MM2-4, respectively. There is no morphological reason to expect them to have solidified under significantly different conditions and together these samples illustrate most clearly the differences that commonly exist between highly magnetic and normally magnetic samples.

The fact that all samples taken from each of the MM lava have roughly the same NRM intensity indicates that the lavas are homogeneous, as is probably not the case with the GF samples.

2.4. Esja samples (LW)

This series was chosen to represent olivine-poor lavas. The series is taken from an area intruded with dikes, and samples were collected at different distances from one of these dikes. The samples used here are taken far from the intrusion where the dike has had negligible effect on the rocks (H.P. Gunnlaugsson, unpublished data). The fact that a dike is nearby can be seen as a problem, but the series shows characteristics that are common with other series, and in this series we have the most complete data on the rocks necessary for the interpretations presented in this paper.

3. Experimental

The Mössbauer spectra presented here were measured at room temperature using conventional constant acceleration drive systems and 10–50 mCi ^{57}Co:Rh sources. Velocities and isomer shifts are given relative to the centre of the spectrum of α-Fe at room temperature. Conventional Mössbauer spectra were measured in transmission geometry using absorbers with ∼50 mg/cm^2 of material in a Plexiglas holder. Conversion electron Mössbauer spectra (CEMS) were recorded in emission geometry by placing the sample on a double sided adhesive conducting tape as the cathode in a parallel plate avalanche detector (Weyer, 1976). Remanence measurements were done with a four-probe fluxgate magnetometer at the University of Iceland. Hysteresis magnetic properties were measured using a 69 Hz vibrating sample magnetometer built at Denmark's Technical University. X-ray diffraction (XRD) spectra were recorded using a Cu tube with Si added as an internal standard and analysed with Rietveld methods. The SEM images presented here were taken in backscatter mode on a CamScan MaXim 2040 instrument. Elemental analysis was made by X-ray fluorescence.

We apply Mössbauer spectroscopy as our tool for the general characterisation of the iron mineralogy of the samples. Similar results could be obtained by X-ray diffraction which, however, would not give as quantitative a picture of the iron oxides. This is due to the similarities between the two spinel phases, maghemite and magnetite, in the XRD spectra, which make it difficult to distinguish quantitatively between them. Furthermore, the major lines of the spinel phase overlap with lines from pyroxenes causing problems when spinel phases are only a minor fraction.

4. Results

The data set produced by our measurements is too extensive to present here as a whole, and we have chosen representative examples that lead to the conclusions derived later. As some of the methods applied in our analysis of the Mössbauer spectra are new, a detailed analysis of the Mössbauer spectra of a representative example from the GF series is presented. The general trends observed in the complete data set are presented as well as representative SEM results and magnetic data.

4.1. Analysis of GF22-1

The Mössbauer spectra are shown in Fig. 2. A single spectrum may be virtually impossible to analyse in order to obtain a meaningful determination of area fractions and hence mineral fractions due to the partial overlap of lines. To deal with this, spectra of different separates, here magnetic and bulk samples, together with a CEMS spectrum of the magnetic separate are analysed simultaneously, by assuming the presence of the same spectral components (position of spectral features and linewidths) in different proportions. In each measurement, some components are enhanced relative to others, and the simultaneous analysis finds a solution that allows for an unambiguous determination of area fractions and hyperfine parameters with relatively small errors.

In the systems used in this study, and specifically in this example, it is possible to determine the presence of seven components in the spectra. These are components due to paramagnetic ferrous iron in pyroxene (Fe, Mg)SiO_3 and/or Ca(Fe, Mg, ...)SiO_3, olivine (Fe, Mg)$_2SiO_4$ and ilmenite $FeTiO_3$. Additionally, there is a component due to paramagnetic ferric iron Fe(III) that usually cannot be assigned to a specific mineral phase, although Fe(III) in pyroxene is the most likely origin of this component. Of magnetic minerals the presence of three different components can be determined. The line observed at $v = 6.8$ mm/s is characteristic for the lowest-velocity resonance line from the B site sextet of magnetite (Fe_3O_4) originating from Fe(II) and Fe(III) on octahedral sites, rapidly exchanging electrons at the

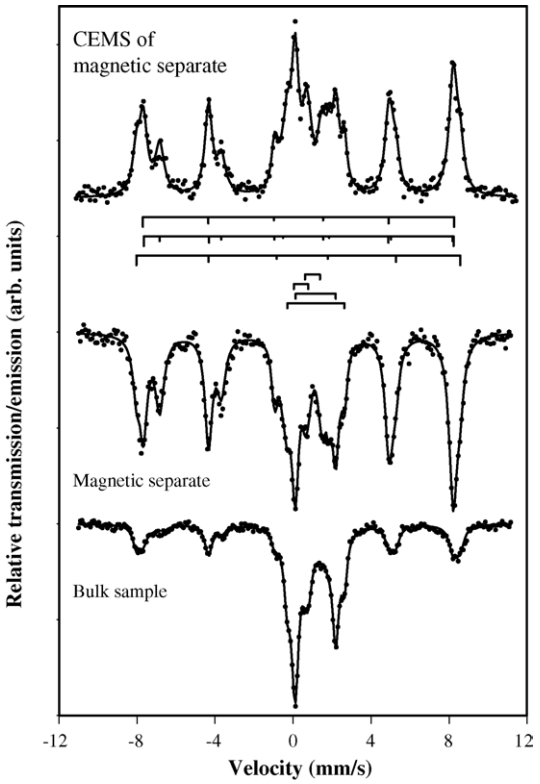

Fig. 2. Room temperature Mössbauer spectra of sample GF22-1 from the GF series. The solid lines are the sum of the fitting components indicated with a bar diagram, from top to bottom: maghemite, magnetite, hematite, ilmenite, Fe(III), Fe(II) in pyroxene and Fe(II) in olivine. The spectra shown are: (bottom) transmission spectrum of the bulk sample, (middle) transmission spectrum of a magnetic separate and (top) CEMS spectrum of the magnetic separate.

timescale of Mössbauer spectroscopy, which results in one sextet component with an isomer shift corresponding to valence state of 2.5+. The presence of this component implies the presence of the A site sextet of magnetite originating from ferric iron on tetrahedral sites with slightly higher magnetic hyperfine field. The area ratio (B/A) between these two components is close to 2, which is clearly not the case in the spectra in Fig. 2. This is due to the presence of sextets from both hematite (α-Fe_2O_3) and maghemite (γ-Fe_2O_3). Due to the rather similar hyperfine parameters of these two components they overlap significantly. However, applying the restriction that hematite has additionally a quadrupole shift ΔE_Q (=2ε) of −0.2 mm/s while the quadrupole shift of maghemite is zero, it is possible to obtain a meaningful determination of area fractions and parameters of these components. The hyperfine parameters and area fractions are gathered in Table 1.

In this example, the area fraction of magnetite is too small and its lines overlap significantly with other lines to allow the determination of hyperfine parameters, therefore literature values were applied (e.g. Greenwood and Gibb, 1971).

The hyperfine parameters of the different components determined from this analysis are generally in good agreement with literature data and allow for their unambiguous assignments (see e.g. Greenwood and Gibb, 1971 and references therein). The details of the pyroxene cannot be determined, and this component probably represents a mixture of clino and orthopyroxene and the two crystallographic sites (M1 and M2) as is evident from larger linewidth in comparison with the olivine. The quadrupole splitting of the olivine falls within the range expected for that phase and suggests the composition Fo_{60} (i.e. 60% forsterite (Fo:Mg_2SiO_4) and 40% fayalite (Fa:Fe_2SiO_4)). The relatively large linewidth of the Fe(III) component suggests that it represents more than one mineral, or that the mineral responsible is not well crystallised. Both possibilities lead to a broadening of the lines.

Table 1
Hyperfine parameters and area fractions obtained from simultaneous analysis of the spectra in Fig. 2

	Magnetite-A	Magnetite-B	Hematite	Maghemite	Pyroxene (2+)	Olivine (2+)	Fe(III)	Ilmenite
B_{hf} (T)	49.2	46.5	51.46(8)	49.5(1)				
δ (mm/s)	0.29	0.67	0.374(7)	0.282(9)	1.158(4)	1.164(5)	0.41(1)	1.00(2)
ΔE_Q (mm/s)	0	0	−0.2	0	2.059(9)	2.93(2)	0.73(2)	0.78(3)
Γ_{16} (mm/s)	0.46(3)	0.53(5)	0.43(5)	0.52(6)	0.42(2)	0.33(2)	0.51(3)	0.40(5)
Γ_{34} (mm/s)	0.33(3)	0.37(4)	0.30(4)	0.37(5)	0.42(2)	0.33(2)	0.51(3)	0.40(5)
A_{bulk} (%)	12(2)	12(2)	12(2)	8(2)	32(2)	11.6(8)	19.1(9)	4.0(6)
A_{mag} (%)	38(3)	38(3)	11(2)	17(3)	14.8(8)	5.8(5)	6.9(6)	4.7(6)
A_{CEMS} (%)	31(2)	31(2)	12(2)	18(2)	13.9(7)	6.3(5)	11.3(7)	5.0(6)
A_{mag}/A_{bulk}	3.1(4)	3.1(4)	1.10(2)	2.1(5)	0.46(3)	0.50(6)	0.36(4)	1.2(3)
A_{CEMS}/A_{mag}	0.82(7)	0.82(7)	1.1(2)	1.1(2)	0.94(7)	1.1(2)	1.6(2)	1.1(2)

The numbers in the parentheses represent 1σ coupled error in the last digit. Parameters with omitted errors were not included as fitting variables. Labels used are: B_{hf}, magnetic hyperfine field; δ, isomer shift; ΔE_Q, quadrupole shift (=2ε) or splitting; Γ, linewidth, for sextets only the linewidths of the inner lines (3 and 4) and outer lines (1 and 6) is presented.

Table 2
Determined weight percentages of iron containing minerals in the bulk sample of GF22-1

Spectral component	f at room temperature	Determined quantity	Values (wt.%)
Hematite	0.84	α-Fe_2O_3	1.7(2)
Maghemite	0.84	γ-Fe_2O_3	1.1(3)
Magnetite	0.83	Fe_3O_4	1.7(2)
Olivine	0.74	Fe(II) in olivine	1.10(8)
Pyroxene	0.72	Fe(II) in pyroxene	3.2(2)
Fe(III)	0.87	Fe in paramagnetic ferric compounds	1.56(8)
Ilmenite	0.65	$FeTiO_3$	1.2(2)

The Debye Waller factors (f) applied are given for reference.

The area ratios show expected tendencies. The area ratios of the highly magnetic phases (maghemite and magnetite) show an increase in the magnetic separate. The paramagnetic silicates show a decrease in area fractions whereas hematite and ilmenite show relatively small changes. This suggests a close association of these phases with the highly magnetic particles. Hematite is pulled out in the magnetic separate as it is found in partly oxidised/inverted particles of magnetite and maghemite, and ilmenite as it is found in fine-grained lamellar-like structures with the magnetite resulting from the solvus exsolution of the original titanomagnetite.

The area fractions are not directly proportional to the number of iron atoms in the different phases, and the Debye Waller factor, f, for the different minerals must be taken into consideration (see e.g. De Grave and Van Alboom, 1991). If the Mössbauer measurements are performed on thin absorbers, this procedure gives the amount of iron in the different mineral phases with good accuracy.

Often the amount of magnetic phases in basalt is minor (<1 wt.%) and in such cases, the lines show up as minor features on the flanks and it may require unrealistically long measuring times to get a reliable determination of area fractions. In such cases thick absorbers are used which, however, leads to thickness effects that generally lead to underestimation of paramagnetic phases and it can be difficult to take these into account in the analysis in a quantitative way. By making the absorbers for Mössbauer spectroscopy thin enough, it is possible to predict the saturation magnetisation of the sample with high accuracy using the room temperature values of saturation magnetisation of $\sigma_S = 90$, 70 and 0.4 A m^2/kg for magnetite, maghemite and hematite, respectively. Conversely, the relative area fractions determined from the analysis of spectra of thick absorbers can be used in conjunction with saturation magnetisation measurements to deduce how much the paramagnetic phases are underestimated in the measurements of thick absorbers to obtain a quantitative picture of the iron mineralogy.

Based on the methods described above, the elemental composition (9.5(1) wt.% Fe) and saturation magnetisation measurements ($\sigma_S = 2.363(7)$ A m^2/kg), weight percent of the seven components are calculated and results are presented in Table 2.

4.2. General trends

The quantitative analysis of the iron mineralogy, as detailed above with sample GF22-1, is powerful enough to allow for the observation of general trends in the data. Fig. 3 presents the NRM intensity of different series of samples as a function of the amount of iron in highly magnetic phases (i.e. magnetite and maghemite).

In all cases, it appears that olivine basalt possesses some special properties in this context. While the NRM intensity is found to increase roughly linearly up to approximately 1.5 wt.% of highly magnetic phases, the

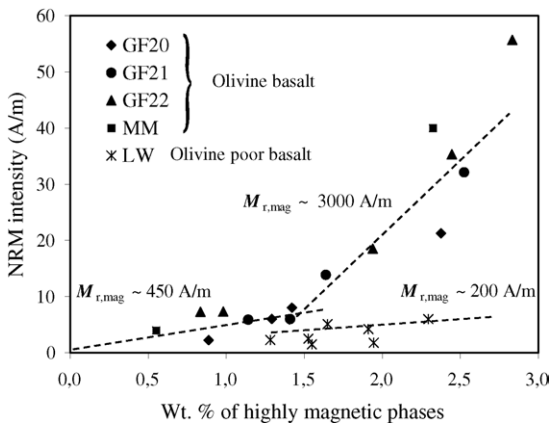

Fig. 3. Remanent magnetisation as a function of amount of highly magnetic phases (magnetite and maghemite) for several series of samples. Stardalur averages are at 5 wt.% highly magnetic phase and $M_r = 61$ A/m. The $M_{r,mag}$ values indicate the remanent magnetisation of the highly magnetic phase necessary to explain the slope. These numbers depend slightly on the assumption of densities. Errors in weight percentage of highly magnetic phases are not included for clarity, but are of the order of 0.2 wt.%.

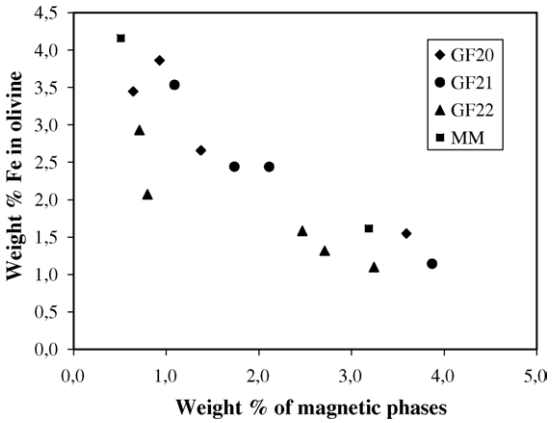

Fig. 4. Weight percentage of Fe in olivine as a function of weight percentage of Fe in magnetic phases (i.e. magnetite, maghemite and hematite) as determined by Mössbauer spectroscopy and elemental analysis for the sample series indicated. Errors are not included for clarity, but are of the order 0.2 wt.%.

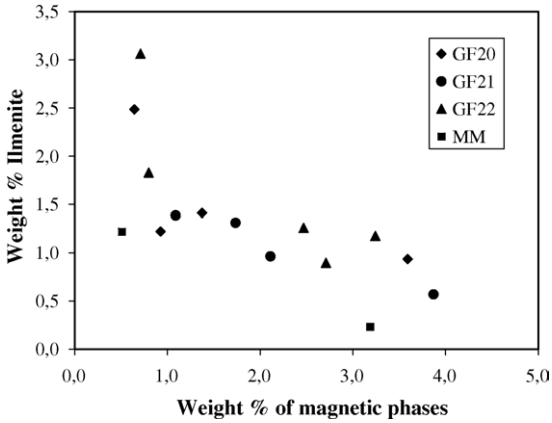

Fig. 5. Weight percentage of ilmenite as a function of weight percentage of Fe in magnetic phases as determined by Mössbauer spectroscopy and elemental analysis for the sample series indicated. Errors are not included for clarity, but are of the order 0.2 wt.%.

curve seems to break, and the NRM intensity increases at a higher rate above that value as a function of highly magnetic phases. As the fraction of highly magnetic phases is used to compile the data illustrated in Fig. 3, a very similar comparison is obtained by using the saturation magnetisation. The scattering of data increases if all magnetic phases (addition of hematite) are included, indicating that hematite does not contribute significantly to the NRM. Similar increased scattering of points is seen if either only the amount of maghemite or magnetite is used. The high slope of the olivine basalt curve is consistent with the presence of SD magnetite/maghemite while in the case of the LW samples the NRM is as expected for MD particles.

The amount of iron in olivine is found to correlate with the amount of magnetic phases as is shown in Fig. 4. This suggests that during solidification, there has been a competition between the magnetic phase and the olivine for iron. The simplest explanation, based on the experimental work of Haggerty and Baker (1967), is a symplectic exsolution of olivine during cooling of the basalt leading to the formation of magnetite.

Similar, but not as clear is the correlation between ilmenite and the magnetic phase as shown in Fig. 5. Such a relationship would result from the process of solvus exsolution, in which an intergrowth of nearly-pure magnetite and ulvöspinel-rich titanomagnetite is formed, with the latter oxidising to ilmenite according to:

$$\underset{\text{(titanomagnetite)}}{6\,Fe_{3-x}Ti_xO_4} + xO_2 \rightarrow \underset{\text{(magnetite)}}{(6-4x)Fe_3O_4} + \underset{\text{(ilmenite)}}{6xFeTiO_3} \quad (1)$$

Higher ilmenite/magnetite ratios suggest higher values of x in the original titanomagnetite, and lower oxidation state of the parent magma (see e.g. Frost, 1991).

4.3. SEM results

There are characteristic differences in the SEM images of highly- and normally-magnetic samples from each series. We shall use the data from the MM series to compare these differences, and for comparison show data from a Stardalur sample. SEM images of samples from the GF series show similar features, but different samples show different results, probably originating from the fact that the samples are very heterogeneous and only small fraction of the whole sample is viewed under the microscope, not necessarily typical for the whole sample.

The MM samples have indistinguishable chemistry, but differ by an order of a magnitude in NRM intensity. The highly magnetic MM2-4 has an NRM intensity of 40 A/m while the more regular MM1-4 has an NRM intensity of 4 A/m. The saturation magnetisation of the bulk samples at room temperature is 1.99(2) and 0.469(3) A m^2/kg for MM2-4 and MM1-4, respectively, suggesting roughly four times greater amount of highly magnetic phases in MM2-4 relative to MM1-4. The Mössbauer parameters of the olivine component are identical, and the position of d301 line from X-ray diffraction is 2.799(2) Å for both MM2-4 and MM1-4 suggesting Fo_{60} average composition of the olivine in both cases.

Fig. 6 shows an electron microscope image of sample MM1-4 taken in backscatter mode. The olivines (type C

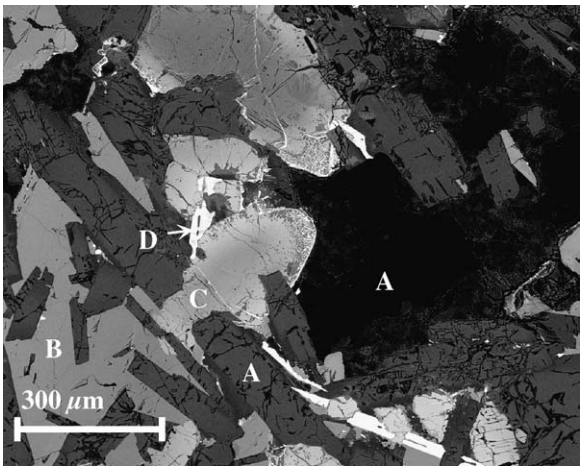

Fig. 6. SEM backscatter image of MM1-4. The sample is dominated by darkish particles (marked A) of feldspar, greyish particles (marked B) of pyroxene, olivine particles (marked C) which are characteristically darker in the middle and lighter at the edges and Fe–Ti oxide phases (marked D).

in Fig. 6) are generally easily distinguished in the images as they show a characteristic composition gradient from Mg rich olivine in the centre to Fe rich olivine at the edges. Fig. 7 shows a more detailed image of the olivine particle seen in the middle of Fig. 6. The particle is more Mg-rich in the centre, indicating higher solidification temperature when it has started precipitating. Apparently, some of the iron exsolved by oxidation from the olivine has migrated out to the edge of the crystal (diffusion rims) whereas some iron remains as exsolution patches of iron oxide within the grain. Analysis of individual grains of these iron oxides (by energy dispersive

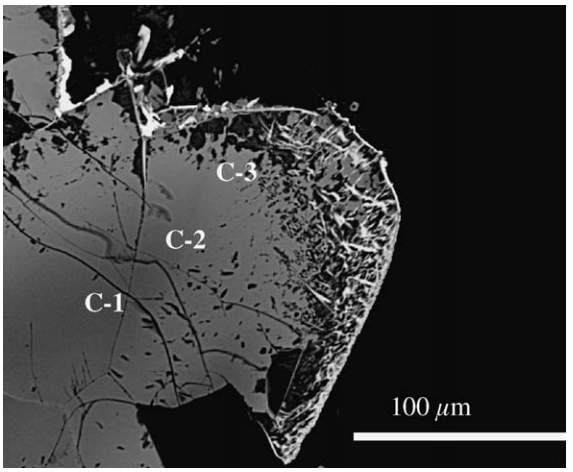

Fig. 7. SEM backscatter image of the olivine particle in the centre of Fig. 6. Three spots marked (C-1 to C-3) were analysed, giving Mg/(Fe + Mg) ratio of 0.70, 0.67 and 0.55 for C-1 to C-3, respectively.

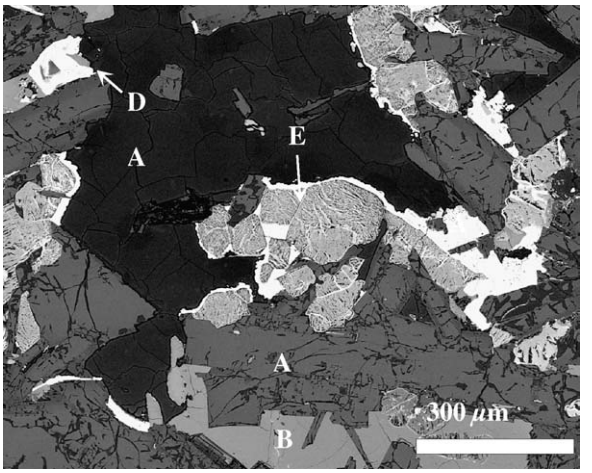

Fig. 8. SEM backscatter image of MM2-4. Some of the same types of particles are found as in the case of MM1-4, i.e. feldspars (A), pyroxenes (B) and Fe–Ti oxides (D). Particles of pure olivine composition are replaced by another type, here marked (E).

spectroscopy X-ray microanalysis) is hampered by their small size (analysed size ∼1 μm), but, the fact that no titanium is present there proves their origin by oxidation and exsolution from the olivine.

Fig. 8 shows an electron-microscope image of sample MM2-4 taken in backscatter mode. Despite intensive search, no particles of olivine composition similar to the ones in the weakly magnetic sample MM1-4 (Fig. 6) were found. Still both the Mössbauer spectroscopy and X-ray diffraction results show that these particles exist. The most obvious candidates are the particles marked E in Fig. 8. Fig. 9 shows a close-up image of such a particle. The internal structure of the particles of type E, shows lamellar-like structures with voids. The close-up image shows that these lamellae consist at least of two

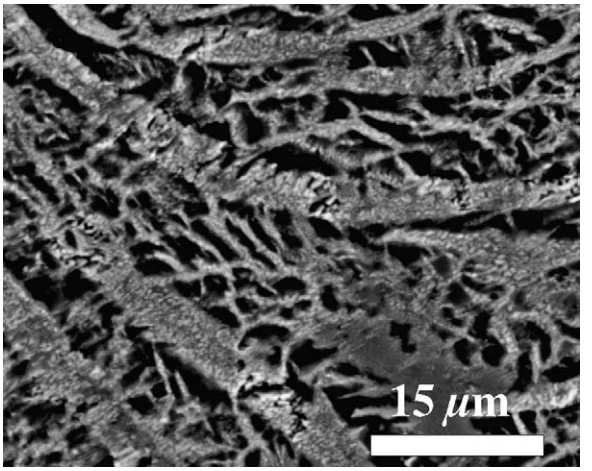

Fig. 9. SEM backscatter image of a particle of type E in Fig. 8.

types of particles. Several analyses were attempted, and all showed only the elements Mg, Fe and Si (oxygen could not be determined) in variable amounts. The Si content was found to scatter between 35 and 44 at.% for different 1 μm spots, neither consistent with pure olivine (33 at.% Si) nor pyroxene (50 at.%). When viewed under the microscope in reflected light, at least some of the particles of type E showed up reddish and with high silvery reflectivity on the polished surface, indicating the presence of hematite.

If we are to conclude that the particles of type E are the source of the (almost stoichiometric) olivine indicated by XRD and Mössbauer spectroscopy, the elemental analyses indicate that other silicates than olivine must be present in the sample as well, especially orthopyroxene or quartz as submicron particles. In particular, the former component could easily be present in the XRD data but is not identifiable. The Lorentzian broadening of the XRD lines of olivine suggests crystal sizes of 120(20) and 50(30) nm, in MM1-4 and MM2-4, respectively. While this broadening is probably caused by compositional variation in MM1-4, an additional broadening in MM2-4 could be caused by the nanometer scale olivine in the structures indicated in Fig. 9.

The particles of type E show similar iron oxide diffusion rims to the particles of type C, only more pronounced. The only features in MM1-4 that remotely resemble those of particles of type E, are the oxide fronts, where iron oxide phases seem to be getting embedded into the olivine crystals.

These features have been seen in different samples, but may differ in morphology and texture from sample to sample. Fig. 10 shows a similar feature in a Stardalur sample. Here, the iron oxide is found in two different forms: As 20–200 μm Fe–Ti oxides (marked D), showing typical exsolution lamellae of ilmenite/magnetite when the contrast of the images is enhanced (inset in Fig. 10). And also as small iron oxides, with no titanium, mixed into areas of voided structures (marked E). As in the case of the MM samples, no typical large olivine particles (type C) were found. No obvious diffusion rims are seen in this example. Still, the small titanium free iron oxide particles show generally higher population on the edges of E type areas.

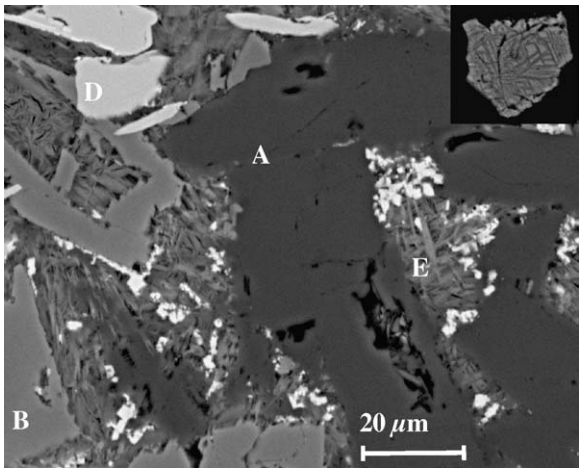

Fig. 10. SEM backscatter image of a Stardalur sample (STI-60). The same types of particles are observed as in the case of the MM2-4 sample. The main difference between the type E particles here in comparison to the M2-4 sample is that the iron oxides are larger and clearly identified here. Analyses revealed that the iron oxides in areas of type E contain no titanium. The inset picture in the upper right corner shows a contrast enhanced image of a Fe–Ti particle of type D.

4.4. Hysteresis properties

It is possible to obtain more information of the magnetic structure of the samples by means of hysteresis measurements, and the comparison of magnetic properties of different magnetic separates. Table 3 lists the magnetic data of a sample from Stardalur. Despite considerable effort the magnetic separation was not very successful as seen in the relatively high saturation magnetisation of the rest fraction; 74(3)% of the bulk value (100% corresponds to no fractioning at all and 0% to perfect fractioning). This is a non-quantitative parameter, as it depends on the effort put into the magnetic separation and the particle size of the powder sample. However, as the preparation procedure of the samples was identical in all cases, experience allows for qualitative characterisation of samples. Obtaining rest fractions

Table 3
Hysteresis data of the sample STI-60

Sample STI-60	σ_S (A m^2/kg)	$\mu_0 H_c$ (T)	σ_r (A m^2/kg)	σ_r/σ_S
Bulk	5.2(2)	0.017(2)	1.0(2)	0.20(3)
Magnetic separate	16.5(4)	0.0069(6)	1.6(2)	0.10(2)
Rest fraction (non-magnetic)	3.86(9)	0.0184(7)	0.79(5)	0.21(2)

Labels used in the table are: σ_S, saturation magnetisation; $\mu_0 H_c$, coercivity; σ_r, saturation remanence (remanence obtained at $B = 0$ T after saturation at $B = 1.25$ T) and σ_r/σ_S, reduced saturation remanence.

Table 4
Hysteresis data of the MM samples

Sample	σ_S (A m^2/kg)	$\mu_0 H_c$ (T)	σ_{Sr} (A m^2/kg)	σ_{Sr}/σ_S
MM1-4, bulk	0.469(7)	0.0187(7)	0.076(4)	0.162(8)
MM1-4, rest	0.265(4)	0.0236(5)	0.053(2)	0.200(7)
MM2-4, bulk	1.99(3)	0.0376(6)	0.70(3)	0.35(2)
MM2-4, rest	1.66(3)	0.0377(6)	0.63(2)	0.38(2)

Hysteresis properties of magnetic separates were not obtained.

with lower relative saturation magnetisation than the bulk sample is the common case (45% on the average for LW samples). This can be explained by examining Fig. 10: the crushing of the sample leads to average particle sizes of ∼50 μm. The most magnetic particles that are pulled out have also a size distribution around this value. Particles that are intimately mixed into the olivine contain only relatively small fraction of iron oxides are thus not as easily extracted in this process. The particles in the magnetic separate show lower coercivity and reduced saturation remanence indicating more MD magnetic properties while these values remain unchanged in the rest fraction.

Table 4 shows the hysteresis properties obtained on the MM samples. The same tendencies are observed as in the case of the Stardalur sample, indicating that the nonmagnetic fractions contain particles with more pronounced SD properties, and that the separation was more difficult in the case of the highly magnetic samples.

Usually a direct correlation between coercivity values and NRM intensity is not found. This is probably due to the fact that the ilmenite/magnetite structures formed during ageing and alteration may be on the submicron scale, leading to pseudo-SD magnetic properties. Only in samples containing titanomagnetite with $x \sim 0.2$, i.e. where no solvus exsolution has taken place, a clear correlation can be observed. This allows us to suggest that it is indeed the small particles mixed into the olivine that give rise to the high NRM intensity of the basalt, and not the Fe–Ti oxide phases.

4.5. CEMS spectra

It still needs to be demonstrated that the voided structures (type E) seen in highly magnetic samples contain olivine. The CEMS spectra give the clearest indication for this. Since the conversion electrons released in the decay of the 14.4 keV state of ^{57}Fe can only penetrate about 0.25 μm of material, CEMS is only sensitive to the surface of the particles. Oxidised areas represent weaknesses in the material and during mechanical breaking of the sample into powder form, it will be more likely to break along these weaknesses, which are thus on the surface of the resulting particles. Owing to the much lower sensitivity range of CEMS as compared to averaging over the whole volume probed in the transmission measurements, the Fe(III) lines are correspondingly more intense in the CEMS measurements as found by Gunnlaugsson et al. (2002). From Fig. 10, it is easy to imagine that the areas of type E represent weaknesses in the structures of the sample that can be exposed during crushing of the samples. Fig. 11 shows a comparison of a transmission Mössbauer spectrum and CEMS spectrum of the sample STI-60. Apart from the not-so-surprising larger fraction of Fe(III) at the surface of the particles, there is evidently a higher amount of olivine in the surface layer of the crushed particles, and the area fraction of olivine increases from roughly 9% to 22%. Thus it seems evident that the areas of type E are associated with the presence of olivine. In this particular case, the quadrupole splitting of the olivine was found to be very

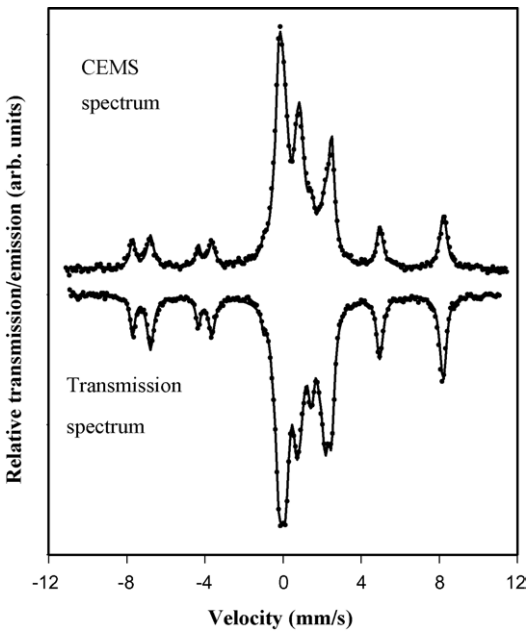

Fig. 11. CEMS spectrum and transmission Mössbauer spectrum of a sample from Stardalur (STI-60) recorded at room temperature.

low for olivine, suggesting admixture with Fe containing serpentine.

Defining κ as the area ratio between the Mössbauer lines of olivine and pyroxene (A_{Ol}/A_{pyr}) in the surface sensitive measurement relative to the bulk measurement $\kappa = (A_{Ol}/A_{pyr})_{CEMS}/(A_{Ol}/A_{pyr})_{TMS}$ we observe a clear distinction between samples containing particles of type E in SEM measurements and of high NRM intensity, as values of κ between 2 and 3 are usually observed ($\kappa = 2.7(1)$ in the case of the Stardalur sample in Fig. 11), while samples without such particles have κ around unity (Rasmussen et al., 2006). Thus, Mössbauer spectroscopy seems to be able to determine whether the oxidation of olivine has taken place at high temperature.

5. Discussion

Olivine is unstable at both low and high temperatures, and can oxidise to either hematite or magnetite during solidification (Haggerty and Baker, 1967) or by later stage oxidation (Hoye and Evans, 1975; Hoffmann and Soffel, 1986). The details of the process depend on various parameters, in particular on the original composition of the olivine and different pathways have been described in the literature. One possibility is (Haggerty and Baker, 1967):

$$\underset{\text{(olivine)}}{6FeMgSiO_4} + O_2 \rightarrow \underset{\text{(magnetite)}}{2Fe_3O_4} + \underset{\text{(enstatite)}}{6MgSiO_3} \quad (2)$$

The morphology of particles described from the annealing studies of Haggerty and Baker (1967) as seen under the microscope is very similar to the ones observed here, especially data from high temperature (>800 °C) prolonged annealing studies. In their study, the starting material was Mg rich olivine (Fo_{80}), and they found that enstatite and also pure forsterite was formed. Eq. (2) assumes Fo_{50} composition, and with Mg rich olivine, the formation of forsterite would be favoured. No correlation between NRM intensity and the composition of the olivine was found, neither by means of Mössbauer spectroscopy (i.e. the quadrupole splitting of the olivine spectral component) nor by changes in the lattice constant of olivine as determined by XRD, in samples where the XRD lines of olivine where strong enough to allow for reliable determination. These findings suggest that part of the olivine has reacted, forming silicates that cannot be determined by Mössbauer spectroscopy and not forsterite, while the rest of the olivine is unaltered. Small amounts of enstatite as suggested in Eq. (2) could, due to overlapping of lines, escape detection in XRD.

Based on preliminary data and incomplete analyses we have previously favoured later annealing events as the source of the high NRM intensity (Gunnlaugsson et al., 2003) but the present, more complete data are in contradiction to these interpretations.

5.1. Comparison to data from Mars

Among the major discoveries of the Mars Global Surveyor mission is the finding of strong magnetic anomalies due to crustal remanence (Acuña et al., 1999). Models suggest magnetic rocks of tens of kilometer thickness with remanent magnetisation up to $M_r \sim 20$ A/m (Purucker et al., 2000), about an order of magnitude higher than average values for terrestrial mid-ocean ridge basalt (MORB). Although Fe–Ti oxide phases, as in MORBs, are the obvious candidates for explaining the remanence, other mineralogical explanations have been suggested to account for the high remanence in comparison with MORBs. These include hemo-ilmenite (Robinson et al., 2002), multi-domain (MD) hematite (Kletetschka et al., 2000), and pyrrhotite (Rochette et al., 2001), none of which are common explanations for the magnetic properties of igneous rocks.

In comparison to Mössbauer data from Mars, we limit ourselves to published work on the basaltic rocks at Gusev crater as measured by the Mars exploration rover Spirit (Morris et al., 2004). Based on crater counting the age of these rocks has been estimated to be 3.9 Ga (Hartmann and Neukum, 2000). Mössbauer spectra of the rocks all show a high amount of olivine and the data suggests that they have been mechanically eroded (Morris et al., 2004). Combining the Mössbauer data with elemental analyses (Gellert et al., 2004), it can be estimated that roughly 6.5 wt.% of Fe is in olivine. This is by a factor of two higher than observed in the olivine basalt samples in this study. The Mössbauer spectra show also signs of highly magnetic phases. In the paper by Morris et al. (2004) this is interpreted as being due to non-stoichiometric magnetite, but just as reasonable an explanation would be a mixture of pure magnetite and maghemite in accordance with the interpretations presented here. Together with the elemental analysis, this corresponds roughly to 2–3 wt.% of highly magnetic phases. If the rocks at Gusev crater had solidified in a magnetic field of terrestrial magnitude (~50 μT), one would expect them to carry remanence of 20–40 A/m with reference to Fig. 3. This is indeed the estimated value of remanent magnetisation of Martian surface rocks (Purucker et al., 2000) based on magnetic data (Acuña et al., 1999). Thus we will suggest a conceptually simpler explanation for the presence of magnetic anomalies on Mars, based only on the magnetic properties of terrestrial olivine basalt.

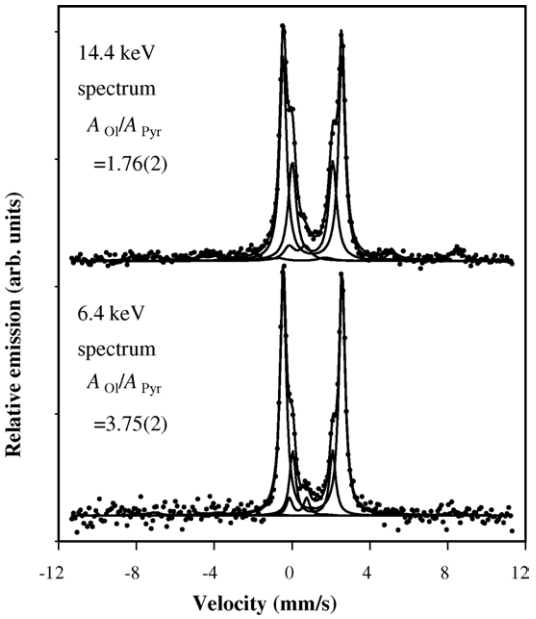

Fig. 12. Mössbauer spectra taken of the rock named Mazatzal on Mars (Spirit Sol 84) after rock abrasion. The spectra are recorded at temperatures ranging from 210 to 270 K (data obtained from the Planetary Data System).

It is not possible to see directly a correlation between the proportion of olivine and that of magnetic phases in the 14.4 keV Mössbauer data from Mars (Morris et al., 2004). This is probably due to the fact that the rocks are not homogeneous as seen in the difference between the 14.4 and the 6.4 keV Mössbauer measurements (sampling depth ~150 and ~75 μm, respectively). Generally the 6.4 keV spectra show increased amount of olivine in comparison to 14.4 keV spectra (cf. Fig. 12). This effect is similar to the difference between CEMS and transmission spectra discussed above, and supports the interpretation that the rocks observed on Mars contain olivine oxidised at high temperatures.

It is noteworthy to add two findings in this context. First, the same difference between olivine and pyroxene ratios is observed on Mössbauer measurements of pristine rock surfaces (i.e. no brushing nor abrasion) supporting the evidence that the erosion at Gusev crater has primarily been mechanically driven. And secondly, if one obtains the interior composition of the rocks by subtracting the analysis results of the 6.4 keV spectra from the analysis results from the 14.4 keV spectra, the expected correlation between olivine amount and iron oxides as in Fig. 4 is observed (Rasmussen et al., 2006).

The rocks at the Gusev landing site have been reported to be considerably weaker physically than typical fine grained basalt (Arvidson et al., 2004). This appears consistent with the weakening of the rocks due to formation of magnetite from oxidation of olivine as was seen here in the SEM images and CEMS measurements, although it is not possible to see a correlation between the magnetite/olivine ratio in Mössbauer measurements and the applied grinding energy.

One characteristic difference between the Mössbauer spectra of the samples used here and the spectra from Gusev crater is the total absence of ilmenite in the Martian spectra. Though it is difficult to determine the presence of ilmenite if it is less than 1 wt.% of the bulk sample, one can estimate that if the magnetic phase in the rocks at Gusev had been titanomagnetite which due to ageing had transformed into pure magnetite and ilmenite, the expected spectral fraction of ilmenite would be of the order of few percent, which should have been visible in the Mössbauer spectra. This is probably due to the extremely small amount of Ti in the rocks at the Gusev landing site (Gellert et al., 2004).

Colour differences between the dust accumulated onto the capture and filter magnets on the MERs (Bertelsen et al., 2004) and investigation of the details in the pattern of particles accumulated onto the capture magnet (Kinch et al., 2006) have revealed that there is a correlation between the colour of the particles and magnetic properties. The most strongly magnetic particles have a darker colour, similar to dust-free rocks (see e.g. McSween et al., 2004), and the more altered bright reddish particles are less magnetic. If the magnetism of the dust was due to oxidised titanomagnetite, the opposite would be anticipated, as the oxidation of relatively weakly magnetic titanomagnetite would lead to the formation of the strongly magnetite/maghemite. It is possible, that while oxidation of titanomagnetite is the dominating mechanism of magnetite formation in basaltic rocks on Earth, the dominating mechanism of magnetite formation on Mars is due to oxidation of olivine.

The interpretations presented here are generally in contradiction to results from studies using Martian meteorites. First of all, the Martian meteorites have mostly a young crystallisation age (<1.2 Ga, apart from ALH84001), and no Martian olivine bearing basaltic shergottite shows the magnetite inclusions (Rochette et al., 2005). This may suggest that the Martian meteorites available are not typical for the oldest rocks on Mars, or that the landing site of Gusev crater does not contain typical rocks.

Mössbauer spectroscopy of the dust accumulated onto the Mars exploration rovers (MER) magnets (Madsen et al., 2003) shows dominantly paramagnetic minerals due to Fe(II) in olivine, pyroxene and Fe(III) (Goetz et

al., 2005), before dust clearing events (Bertelsen et al., 2006). The results have been similar for both MER landing sites and suggest that the dust derived from olivine containing basaltic rocks. The magnets have collected the fine dust suspended in the atmosphere with average diameter of 3 μm (Lemmon et al., 2004) that has probably been homogenised over the entire planet. This indicates that the presence of olivine basalt is not a local phenomenon at Gusev crater and olivine basalt may be much more common on Mars than is inferred from Martian meteorite statistics.

6. Conclusions

It has been shown that olivine basalt can become an order of a magnitude more magnetic than basalt not containing olivine despite the same amount of highly magnetic phases. This is attributed to the partial oxidation of the olivine to pure single domain magnetite of sub-micrometer size. These conclusions are based on detailed studies of Icelandic samples by various techniques, where the mineralogical composition of particles in particular has been deduced from Mössbauer spectroscopy.

Mössbauer spectroscopy at Gusev crater has revealed olivine basalt on Mars and the combination of techniques shows that these rocks have some properties in common with the rocks in this study, allowing us to conclude that at least at Gusev crater there are rocks that could be highly magnetic if they had solidified in a magnetic field of terrestrial magnitude, offering a simple explanation of the magnetic anomalies on Mars.

Based on the findings here and Mössbauer spectroscopy of the magnetic dust circulating in the atmosphere on Mars, it is suggested that olivine basalt is the parent material for the dust, and more common than inferred from Martian meteorite statistics.

Acknowledgements

H.P. Gunnlaugsson acknowledges support from the Danish Natural Science Foundation (2006-01-0030). The late J.M. Knudsen and R.B. Hargraves are acknowledged for fruitful discussions. J. Chevallier at Aarhus University is acknowledged for experimental help.

References

Acuña, M.H., Connerney, J.E.P., Ness, N.F., Lin, R.P., Michell, D., Carlson, C.W., McFadden, J., Anderson, K.A., Rème, H., Mazelle, C., Vignes, D., Wasilewski, P., Cloutier, P., 1999. Global distribution of crustal magnetization discovered by the Mars Global Surveyor MAG/ER experiment. Science 284, 790–793.

Ade-Hall, J.M., Palmer, H.C., Hubbard, T.P., 1971. The magnetic and opaque petrological response of basalts to regional hydrothermal alteration. Geophys. J. R. Astronom. Soc. 24, 137–174.

Arvidson, R.E., Anderson, R.C., Bartlett, P., Bell III, J.F., Blaney, D., Christensen, P.R., Chu, P., Crumpler, L., Davis, K., Ehlmann, B.L., Fergason, R., Golombek, M.P., Gorevan, S., Grant, J.A., Greeley, R., Guinness, E.A., Haldemann, A.F.C., Herkenhoff, K., Johnson, J., Landis, G., Li, R., Lindemann, R., McSween, H., Ming, D.W., Myrick, T., Richter, L., Seelos IV, F.P., Squyres, S.W., Sullivan, R.J., Wang, A., Wilson, J., 2004. Localization and physical properties experiments conducted by Spirit at Gusev crater. Science 305, 821–824.

Becker, H., 1980. Magnetic anomalies (ΔZ) in NE-Iceland and their interpretations based on rock-magnetic investigations. J. Geophys. 47, 43–56.

Bertelsen, P., Goetz, W., Madsen, M.B., Kinch, K.M., Hviid, S.F., Knudsen, J.M., Gunnlaugsson, H.P., Merrison, J., Nornberg, P., Squyres, S.W., Bell III, J.F., Herkenhoff, K.E., Gorevan, S., Yen, A.S., Myrick, T., Klingelhöfer, G., Rieder, R., Gellert, R., 2004. Magnetic properties experiments on the Mars exploration rover Spirit at Gusev crater. Science 305, 827–829.

Bertelsen, P., Madsen, M.B., Binau, C.S., Goetz, W., Gunnlaugsson, H.P., Hviid, S.F., Kinch, K.M., Klingelhöfer, G., Leer, K., Madsen, D.E., Merrison, J.M., Olsen, M., Squyres, S.W., 2006. Backscattering Mössbauer spectroscopy of Martian dust. Hyperfine Interact., in press.

De Grave, E., Van Alboom, A., 1991. Evaluation of ferrous and ferric Mössbauer fractions. Phys. Chem. Miner. 18, 337–342.

Dunlop, D.J., 1990. Developments in rock magnetism. Rep. Prog. Phys. 53, 707–792.

Friðleifsson, I.B., Kristjansson, L., 1972. The Stardalur magnetic anomaly, SW-Iceland. Jökull 22, 69–78.

Frost, B.R., 1991. Magnetic petrology: factors that control the occurrence of magnetite in crustal rocks. In: Lindsley, D.H. (Ed.), Oxide Minerals: Petrology and Magnetic Significance, Reviews in Mineralogy, vol. 25. Mineralogical Society of America, pp. 489–509.

Gellert, R., Rieder, R., Anderson, R.C., Bruckner, J., Clark, B.C., Dreibus, G., Economou, T., Klingelhöfer, G., Lugmair, G.W., Ming, D.W., Squyres, S.W., d'Uston, C., Wanke, H., Yen, A., Zipfel, J., 2004. Chemistry of rocks and soils in Gusev crater from the alpha particle X-ray spectrometer. Science 305, 829–832.

Goetz, W., Bertelsen, P., Binau, C.S., Gunnlaugsson, H.P., Hviid, S.F., Kinch, K.M., Knudsen, J.M., Madsen, D.E., Madsen, M.B., Olsen, M., Gellert, R., Klingelhöfer, G., Ming, D.W., Morris, R.V., Rieder, R., Rodionov, D.S., de Souza Jr., P.A., Squyres, S.W., Wdowiak, T., Yen, A., 2005. Indication of drier periods on Mars from the chemistry and mineralogy of atmospheric dust. Nature 436, 62–65.

Greenwood, N.N., Gibb, T.C., 1971. Mössbauer Spectroscopy. Chapman and Hall, London.

Gunnlaugsson, H.P., Weyer, G., Helgason, Ö., 2002. Titanomaghemite in Icelandic basalt: possible clues for the strongly magnetic phase in Martian soil and dust. Planet. Space Sci. 50, 157–161.

Gunnlaugsson, H.P., Bendtsen, L.S., Bertelsen, P., Binau, C., Gaarsmand, J., Goetz, W., Helgason, Ö., Kristjansson, L., Knudsen, J.M., Leer, K., Madsen, M.B., Nørnberg, P., Steinthorsson, S., Weyer, G., 2003. Magnetic anomalies in Iceland: implications for the magnetic anomalies on Mars. In: Proceedings of the 6th International Conference on Mars, Pasadena (abstract no. 3025).

Haggerty, S.E., Baker, I., 1967. The alteration of olivine in basaltic and associated lavas. Part I. High temperature alteration. Contrib. Mineral. Petrol. 16, 233–257.

Hartmann, W.K., Neukum, G., 2000. Cratering chronology and the evolution of Mars. Space Sci. Rev. 96, 165–194.

Helgason, Ö., Steinthorsson, S., Madsen, M.B., Mørup, S., 1990. On anomalously magnetic basalt lavas from Stardalur, Iceland. Hyperfine Interact. 57, 2209–2214.

Hoblitt, R.P., Larson, E.E., 1975. New combination of techniques for determination of the ultrafine structure of magnetic minerals. Geology 3, 723–726.

Hoffmann, V., Soffel, H.C., 1986. Magnetic properties and oxidation experiments with synthetic olivines $(Fe_xMg_{1-x})_2SiO_4$ $0 \leq x \leq 1$. J. Geophys. 60, 41–46.

Hoye, G.S., Evans, M.E., 1975. Remanent magnetization in oxidized olivine. Geophys. J. R. Astronom. Soc. 41, 139–151.

Jonsson, G., Kristjansson, L., Sverrisson, M., 1991. Magnetic surveys of Iceland. Tectonophysics 189, 229–247.

Kinch, K.M., Merrison, J.P., Gunnlaugsson, H.P., Bertelsen, P., Madsen, M.B., Nørnberg, P., 2006. Preliminary analysis of the MER magnetic properties experiment using a CFD model. Planet. Space Sci. 54, 28–44.

Kletetschka, G., Wasilewski, P.J., Taylor, P.T., 2000. Hematite versus magnetite as the signature for planetary magnetic anomalies? Phys. Earth Planet. Int. 119, 259–267.

Kletetschka, G., Acuna, M.H., Kohout, T., Wasilewski, P.J., Connerney, E.P., 2005. An empirical scaling law for acquisition of thermoremanent magnetization. Earth Planet. Sci. Lett. 226, 521–528.

Kristjansson, L., 1970. Paleomagnetism and magnetic surveys in Iceland. Earth Planet. Sci. Lett. 8, 101–108.

Kristjansson, L., Hardarson, B.S., Audunsson, H., 2003. A detailed paleomagnetic study of the oldest (≈15 My) lava sequences of Northwest Iceland. Geophys. J. Int. 155, 991–1005.

Kristjansson, L., Guðmundsson, Á., 2005. Stratigraphy and paleomagnetism of lava sequences in the Suðurdalur area, Fljótsdalur, Eastern Iceland. Jökull 55, 17–32.

Lemmon, M.T., Wolff, M.J., Smith, M.D., Clancy, R.T., Banfield, D., Landis, G.A., Ghosh, A., Smith, P.H., Spanovich, N., Whitney, B., Whelley, P., Greeley, R., Thompson, S., Bell III, J.F., Squyres, S.W., 2004. Atmospheric imaging results from the Mars exploration rovers: Spirit and Opportunity. Science 306, 1753–1756.

Madsen, M.B., Bertelsen, P., Goetz, W., Binau, C.S., Olsen, M., Folkmann, F., Gunnlaugsson, H.P., Kinch, K.M., Knudsen, J.M., Merrison, J., Nornberg, P., Squyres, S.W., Yen, A.S., Rademacher, J.D., Gorevan, S., Myrick, T., Bartlett, P., 2003. The magnetic properties experiments on the Mars exploration rover mission. J. Geophys. Res. 108, 8069.

Mehegan, J.M., Robinson, P.T., Delaney, J.R., 1982. Secondary mineralization and hydrothermal alteration in the Reydarfjordur drill core, Eastern Iceland. J. Geophys. Res. 87, 6511–6524.

McSween, H.Y., Arvidson, R.E., Bell III, J.F., Blaney, D., Cabrol, N.A., Christensen, P.R., Clark, B.C., Crisp, J.A., Crumpler, L.S., Des Marais, D.J., Farmer, J.D., Gellert, R., Ghosh, A., Gorevan, S., Graff, T., Grant, J., Haskin, L.A., Herkenhoff, K.E., Johnson, J.R., Jolliff, B.L., Klingelhöfer, G., Knudson, A.T., McLennan, S., Milam, K.A., Moersch, J.E., Morris, R.V., Rieder, R., Ruff, S.W., de Souza Jr., P.A., Squyres, S.W., Wanke, H., Wang, A., Wyatt, M.B., Yen, A., Zipfel, J., 2004. Basaltic rocks analyzed by the Spirit rover in Gusev crater. Science 305, 842–845.

Morris, R.V., Klingelhöfer, G., Bernhardt, B., Schröder, C., Rodionov, D.S., de Souza Jr., P.A., Yen, A., Gellert, R., Evlanov, E.N., Foh, J., Kankeleit, E., Gütlich, P., Ming, D.W., Renz, F., Wdowiak, T., Squyres, S.W., Arvidson, R.E., 2004. Mineralogy at Gusev crater from the Mössbauer spectrometer on the Spirit rover. Science 305, 833–836.

Planetary Data System, 2005. http://anserver1.eprsl.wustl.edu.

Purucker, M., Ravat, D., Frey, H., Voorhies, C., Sabaka, T., Acuña, M., 2000. An altitude-normalized magnetic map of Mars and its interpretation. Geophys. Res. Lett. 27, 2449–2452.

Rasmussen, H. R., Gunnlaugsson, H. P., Tegner, C., Kristjánsson, L., 2006. Magnetic properties of Martian olivine basalts studied by terrestrial analogues, Hyperfine Interact., in press.

Robinson, P., Harrison, R.J., McEnroe, S.A., Hargraves, R.B., 2002. Lamellar magnetism in the hematite–ilmenite series as an explanation for strong remanent magnetization. Nature 418, 517–520.

Rochette, P., Lorand, J.-P., Fillion, G., Sautter, V., 2001. Pyrrhotite and the remanent magnetization of SNC meteorites: a changing perspective on Martian magnetism. Earth Planet. Sci. Lett. 190, 1–12.

Rochette, P., Gattacceca, J., Chevrier, V., Hoffmann, V., Lorand, J.-P., Funaki, M., Hochleitner, R., 2005. Matching Martian crustal magnetization and meteorite magnetic properties. Meteoritics Planet. Sci. 40, 529–540.

Sigurgeirsson, Th., 1970. Aeromagnetic survey of SW Iceland. Sci. Iceland 2, 13–20.

Steinthorsson, S., Sigvaldason, G. E., 1971. Skýrsla um bergfræðirannsóknir við Stardal. Science Inst., Univ. Iceland, Report.

Steinthorsson, S., Helgason, Ö., Madsen, M.B., Koch, C.B., Bentzon, M.D., Mørup, S., 1992. Maghemite in Icelandic basalts. Mineral. Mag. 56, 185–199.

Vincent, E.A., Wright, J.B., Chevallier, R., Mathieu, S., 1957. Melting experiments on some natural titaniferous magnetites. Mineral. Mag. 31, 624–655.

Weyer, G., 1976. Application of parallel-plate avalanche counters in Mössbauer spectroscopy. In: Gruverman, I.J., Seidel, C.W. (Eds.), Mössbauer Effect Methodology, vol. 10. Plenum Press, New York, pp. 301–319.